Chemical Engineering Journal 150 (2009) 242–251

Contents lists available at ScienceDirect

Chemical Engineering Journal

journal homepage: www.elsevier.com/locate/cej

An auto-sustainable solid oxide fuel cell system fueled by bio-ethanol Process simulation and heat exchanger network synthesis

Luis E. Arteaga-Perez[a,c,*], Yannay Casas[b], Luis M. Peralta[b], Viatshelav Kafarov[c], Jo Dewulf[d], Pablo Giunta[e]

[a] Centro de Análisis de Procesos, Universidad Central de Las Villas, Carretera a Camajuaní Km 5.5, Santa Clara, c/p 54830, Villa Clara, Cuba
[b] Departamento de Ingeniería Química, Universidad Central de Las Villas, Carretera a Camajuaní Km 5.5, Santa Clara, c/p 54830, Villa Clara, Cuba
[c] Center for Simulation and Control of Processes, Universidad Industrial de Santander, A.A. 678, Cra 27 Cl 9, Bucaramanga, Colombia
[d] Research Group ENVOC, Ghent University, Coupure Links 653, 9000 Ghent, Belgium
[e] Facultad de Ingeniería, Universidad de Buenos Aires, Laboratorio de Procesos Catalíticos, Pabellón de Industrias, Ciudad Universitaria, 1428 Buenos Aires, Argentina

ARTICLE INFO

Article history:
Received 3 December 2008
Received in revised form 23 February 2009
Accepted 24 February 2009

Keywords:
Steam reforming
Heat integration
Fuel cells
Reactor modeling

ABSTRACT

In this paper the simulation and heat integration of a solid oxide fuel cell (SOFC) integrated with an ethanol steam reforming system are carried out. The ethanol reaction is studied using a novel kinetic model reported in a previous work. The system and fuel cell efficiencies are studied under different process conditions, temperature ($723 < T < 873$ K), water to ethanol molar ratio ($3 < R_{AE} < 6$) and fuel utilization coefficient ($0.7 < FUC < 0.9$). The SOFC off gases are mixed and fed to an after burner providing heat to the process. Two heat exchanger networks are designed considering the influence of the fuel utilization coefficient (0.7–0.9) at the cell electrodes. If the SOFC is operated at $FUC < 0.8$ a self sufficient limit could be established, otherwise extra ethanol must be combusted with an overall efficiency penalty. A process flow diagram is proposed in order to obtain a high efficiency and to avoid the use of any external source of energy.

1. Introduction

In recent years, the solid oxide fuel cell (SOFC) running on pure hydrogen or synthesis gas has drawn a great attention, due to its application in distributed power systems. Among the various types of fuel cells the SOFC has many distinctive characteristics such as high efficiency in energy conversion, modularity, environmental compatibility, support internal reforming and water gas reaction, no need of noble materials as electrodes and the high operating temperatures of SOFC (873–1273 K) allow the cogeneration and heat reuse [1–3]. In the present paper the general characteristics of a planar solid oxide fuel cell system are depicted: cells arrangement, account and the fuel utilization coefficient. The operation is carried out using synthesis gas produced in an ethanol steam reforming plant.

The catalytic steam reforming of bio-based alcohols, mainly ethanol, is a new interesting focus based on the environmental compatibility of hydrogen energy when compared with other feedstocks [4]. Ethanol has many advantages as a source of hydrogen, since it is easy to store, handle and transport in a safe way due to its lower toxicity and volatility. In addition, this alcohol can be bio-produced from a wide variety of biomass sources, including sugar cane molasses, lignocelluloses and waste materials from agro-industries [5]. On the other hand, if the fermentation of biomass is used to obtain the bio-ethanol, the total net emissions of CO_2 fundamentally lower than fossils.

Bio-ethanol can be converted into a hydrogen rich gas stream using reforming technologies:

- Steam reforming.
- Partial oxidation.
- Autothermal reforming.

Among the mentioned alternatives, ethanol steam reforming is the most studied due to the higher yield and selectivity level obtained when carried out with a proper catalyst. Nevertheless, the energy efficiency is limited due to the high endothermic character of this reaction and the heat losses in the other process stages [5–8]:

$$C_2H_5OH + 3H_2O \rightarrow 2CO_2 + 6H_2 \qquad \Delta H^\circ = +173.5\ \text{kJ mol}^{-1}$$

The high dependence of the reaction pattern with the catalytic formulation and the uncertainty of the existing kinetic models, have

* Corresponding author at: Centro de Análisis de Procesos, Universidad Central de Las Villas, Carretera a Camajuaní Km 5.5, Santa Clara, c/p 54830, Villa Clara, Cuba. Tel.: +53 422 81164; fax: +53 422 81608.
E-mail address: luiseap@gmail.com (L.E. Arteaga-Perez).

1385-8947/$ – see front matter © 2009 Elsevier B.V. All rights reserved.
doi:10.1016/j.cej.2009.02.032

Nomenclature

ac	single cell surface (cm^2)
A_c	SOFC stack surface (cm^2)
A_{tc}	heat transfer area (m^2)
$f^{in}_{H_2}$	hydrogen flow entering in the cell (kmol s^{-1})
$f^{in}_{CH_4}$	methane flow entering in the cell (kmol s^{-1})
$f^{out}_{H_2}$	hydrogen flow in the SOFC exhaust (kmol s^{-1})
F	Faraday constant (96487 C mol^{-1})
F_H	hydrogen flow exiting the reactor (kmol s^{-1})
F_j	outlet molar flow of component j (kmol s^{-1})
F_{jo}	inlet molar flow of component j (kmol s^{-1})
$F^{Eq}_{H_2}$	hydrogen flow produced at equilibrium conditions (kmol s^{-1})
$F^{in}_{ethanol}$	ethanol flow feed to the reactor (kmol s^{-1})
F^{in}_{water}	water flow feed to the reactor (kmol s^{-1})
$F^{out}_{ethanol}$	ethanol flow leaving the reactor (kmol s^{-1})
F^{out}_{water}	water flow leaving the reactor (kmol s^{-1})
$F^{Post\text{-}comb}_{ethanol}$	ethanol flow to the burner (kmol s^{-1})
FUC	fuel utilization coefficient
ΔG	Gibbs free energy of the electrochemical reaction (kJ mol^{-1})
HHV	higher heating value (kJ $kmol^{-1}$)
I_{cell}	cell current (A)
j	subvolume element
J	current density (A m^{-2})
J_l	limit current density (A m^{-2})
$J_{o,i}$	exchange current density (A m^{-2})
LHV	lower heating value (kJ $kmol^{-1}$)
N_{cell}	number of cell in the stack
P_{cell}	cell power output (kW)
P_{H_2}, P_{H_2O}, P_{O_2}	partial pressure of hydrogen, water and oxygen (atm)
Q	heat duty (kW)
R	universal gas constant (J K^{-1} mol^{-1})
R_{AE}	water/ethanol molar ratio
S_{SOFC}	SOFC area (m^2)
t	time (s)
T^{in}_g, T^{out}_g	temperature of hot gases (K)
U	overall heat transfer coefficient (tubes) (kW m^{-2} K^{-1})
V	reactor volume (m^3)
V_{cell}	single cell voltage (V)
V_{ideal}	Nerst potential (V)
W_{comp}, W_{pump}	power of pump and compressor (kW)
X_{CH_4}	methane conversion in the fuel cell
Y_H	hydrogen yield (kmol of produced H_2/kmol of ethanol fed to the reactor)

Greeks letters

η_{act}	activation overpotential (V)
η_{cell}	fuel cell efficiency (%)
η_{conc}	concentration overpotential (V)
η_{esr}	reforming energy efficiency (%)
η_{ref}	reaction efficiency (%)
η_{sys}	system efficiency (%)

affected the process optimization and the system synthesis using robust techniques. In the present paper a validated kinetic model [6] and a modular sequential process simulation are used to simulate and design the heat exchanger network.

Few works have addressed the synthesis of heat exchanger networks for fuel cells coupled to ethanol processors [9–12]. Douvartzides et al. [13] developed an energy–exergy analysis in order to optimize the operational conditions of a SOFC power plant, considering only the hydrogen oxidation within the fuel cell and rejecting the effect of the secondary CH_4 reforming and CO conversion and the losses at the fuel cell electrodes. Moreover, Douvartzides et al. [13] did not take into account the effect of the kinetic pattern of the ethanol steam reforming on synthesis gas composition and however they use the extent of the reaction (ε). The optimal condition was reached for a SOFC fuel utilization factor of 79.85%, an ethanol conversion of 100%, water to ethanol ratio 3:1 and no energy integration technique was used. In a later work Douvartzides et al. [14] applied the method of exergy analysis to a SOFC power plant involving the steam reforming of ethanol and/or methane proving that the reforming extent, fuel utilization and the combustion processes play an important role in the optimization of the system efficiency.

Tsiakaras and Demin [15] consider the thermodynamic equilibrium products of ethanol, (a) steam reforming, (b) reforming with CO_2 and (c) partial oxidation with air, to feed a SOFC. The best performance is exhibited when the electrochemical section is fed with ethanol steam reforming products. The effect of the fuel cell irreversibility on system efficiency and the effect of coke deposition were not reported. The carbon deposition boundaries in a SOFC fed directly with dry ethanol was studied by Cimenti and Hill [16], they report that at low FUC the coke deposition is thermodynamically feasible in a wide range of operation temperature (800–1100 K).

Francesconi et al. [9] analyzed the integration of an ethanol processor with a PEMFC using a thermodynamic approach to study the ethanol reaction and no synthesis of the heat exchanger network was carried out. A similar work was reported by Giunta et al. [10] who propose a heat exchanger network to use efficiently the heat in an ethanol processor, but no energy integration technique is used and the ethanol steam reforming equilibrium is assumed. Song et al. [17] investigated an integrated ethanol fueled PEMFC by exergy analysis.

In a previous work the SOFC plant simulation was carried out without considering the HEN synthesis, and the system utilities were produced by the combustion of a synthesis gas fraction and a simple model of the cell was implemented [7].

In the present paper, the PINCH technology [18,19] is used to design the heat exchanger network of an ethanol fueled SOFC system. This method uses energy and area targeting between composite curves to determine the optimum temperature difference, ΔT_{opt} of the HEN by considering a combination of investment and utility costs. Also the effect of reaction kinetics of the ethanol conversion on heat recovery potential is evaluated using novel criteria that allow determining the energy equilibrium point. On the other hand, a detailed thermodynamic model for the evaluation of the SOFC is provided. The effect of the fuel cell and the reforming operational parameters (reactor temperature, reactants ratio and fuel utilization coefficient) on the plant performance and HEN design is studied.

The mathematical processing of the models is carried out using the Aspen–Hysys® general purpose modeling-environment.

2. Plant analysis. Systematic procedure

2.1. Process flow diagram

Fig. 1 shows a schematic of a SOFC system coupled to an ethanol steam reforming unit. It consists of a mixture preparation section which comprises pumps, a blending tank, a vaporizer and a heater. Here the water/ethanol mixture is prepared to be fed into the reforming reactor at the specific reaction conditions (T, R_{AE}). The

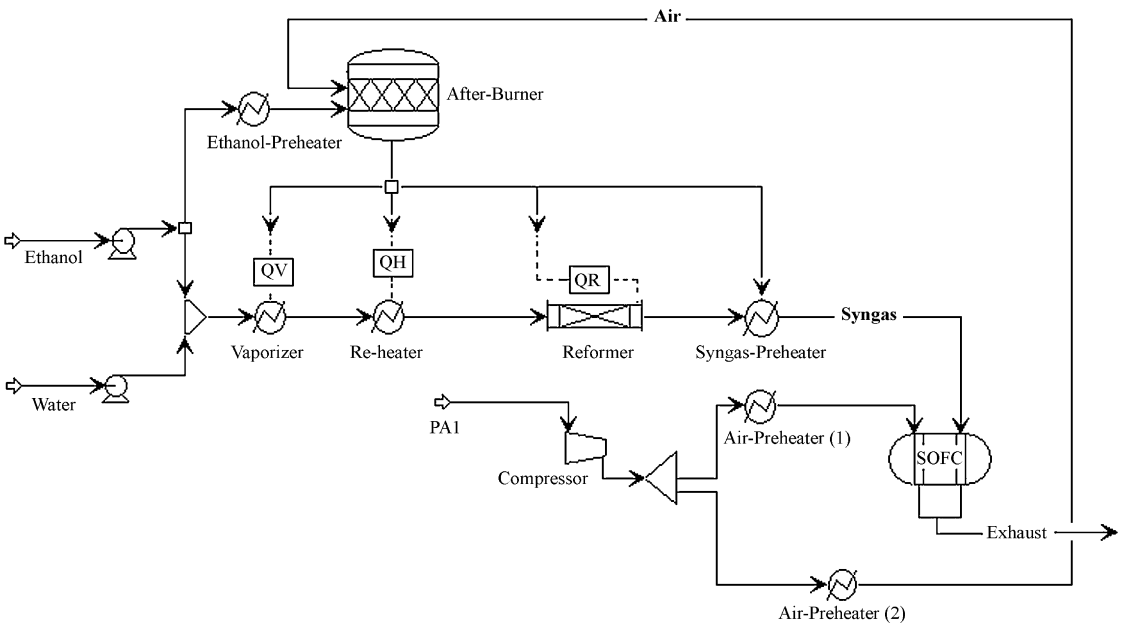

Fig. 1. Schematic of the system base process ESR–SOFC.

steam reformer reactor and re-heater are used to obtain hydrogen rich gas stream ready to be fed into a SOFC fuel cell stack. The SOFC converts the fuel (CH_4, H_2) energy into heat and electric power.

The system is evaluated to produce up to 700 kW of electrical power. The initial flows of hydrogen and ethanol are calculated starting from the correlations of continuous current and the Faraday's law, assuming a cell voltage of 0.6 V and an efficiency of 40.5% [3]:

For a parallel arrangement:

$$I_{cell} = \frac{P_{cell}}{V_{cell}} \quad (1)$$

And considering the fuel utilization coefficient effect, the necessary theoretical hydrogen is:

$$F_H = (A)\left(\frac{1\,C\,s^{-1}}{1\,A}\right)\left(\frac{1\,mol\,e^-}{96487\,C}\right)\left(\frac{1\,mol\,H_2}{2\,mol\,e^-}\right)\left(\frac{3600\,s}{1\,h}\right)\left(\frac{1}{FUC}\right)$$

$$= mol/h$$

The yield approach reported by Fierro et al. [20], Eq. (2) is used to obtain the quantity of ethanol to feed the reforming stage.

$$Y_H = \frac{F_H}{F^{in}_{ethanol}} \quad (2)$$

The approximations mentioned previously are merely used for the initial guess, because both, the system simulation and integration are trial and error procedures. If the flows of hydrogen and ethanol are fixed the system indicators could lead with high deviations of the real behavior and the heat exchanger network synthesis can fail.

Due to the high endothermic character of the ethanol steam reforming (ESR) reaction (ΔH = +173.5 kJ mol^{-1}), heat must be supplied into the system to fulfill the needs of energy in the preparation and the reforming reaction stages. Usually this heat is obtained by the combustion of a fraction of fuel in a burner. In a previous work this fuel was taken as a fraction of the reformate gas stream and no energy integration was due [7]. In the present paper the fuel cell off gases, are used to balance the energy requirements in the PFD by means of a post-combustion system and a heat exchanger network. If the gases leaving the cell do not meet the energy needs, additional ethanol is burned to complete the balance.

The ethanol, water and air (PA1) depicted in Fig. 1 enter into the system at ambient conditions. The models of the steam reformer, fuel cell and post-combustion system are discussed separately.

2.2. Ethanol steam reforming

The conversion of ethanol is carried out in a reforming reactor involving: decomposition, steam reforming and water gas shift reactions. Previous thermodynamics studies [21,22] show that ethanol steam reforming is feasible to high temperatures (T > 500 K) and in a wide range of water/ethanol molar ratios, producing CH_4, H_2O, CO, CO_2 and H_2 as main species. Other hydrocarbon compounds such as acetaldehyde and ethylene are considered intermediate products, which are quickly converted to more simple molecules at high contact times and temperatures (>673 K). The production of these compounds over Ni and Cu sites was reported by Mas et al. [23] and Mariño et al. [24].

It is well known that the reaction pathway which describes the ESR is highly dependent on the operational conditions, the catalyst formulation and the redox characteristic of the support material. The general reaction mechanism can be written as:

$$CH_3CH_2OH + \beta H_2O \rightarrow \text{Products} \quad (3)$$

But the real picture is rather complex; because during the process a series of side reactions take place (ethanol dehydration and decomposition) producing species (CH_3CHO, C_2H_4, CH_3COOH) which competes for hydrogen atoms causing the reduction of the global yield. Therefore, stable and selective catalytic formulations play an important role in the process development.

Among the various reaction patterns previously reported, in the present paper the ESR is analyzed using the approaches showed in Arteaga et al. [7]. This new mechanism includes the ethanol decomposition (Eq. (4)), the water gas shift reaction (Eq. (5)), the methane reforming (Eqs. (6) and (7)), coke deposition and coke conversion (Eqs. (8) and (9)) taking place in a Ni/Al_2O_3 catalyst:

$$CH_3CH_2OH \rightarrow CH_4 + CO + H_2 \quad (4)$$

$$CO + H_2O \rightarrow CO_2 + H_2 \quad (5)$$

$$CH_4H_2O \rightarrow CO + 3H_2 \quad (6)$$

$$CH_4 + 2H_2O \rightarrow CO_2 + 4H_2 \quad (7)$$

$$2CO \rightarrow C + CO_2 \quad (8)$$

$$C + H_2O \rightarrow CO + H_2 \quad (9)$$

The use of this pathway in conjunction with a Langmuir–Hinshelwood kinetic model based on the mechanistic description of all reaction steps, allows obtaining a detailed concentration profile at the reactor outlet and defining the potential for energy savings considering the contribution (LHV, HHV) of each component in the reformate gas [7].

The reactor model is assumed as a bank of cylindrical tubes charged with spherical (0.1 cm) pellets of Ni–Al catalyst. The flow field is modeled as plug flow, that is to say the stream is isotropic in the radial direction (without mass or energy gradients) and axial mixing negligible (Eq. (10)). This implies that the model do not allows studying the radial internal profiles of temperature and concentration:

$$\frac{dn(z,i)}{dz} = A_t(1-\varepsilon)\sum_i \alpha(i,j)\cdot r(z,i) \quad (10)$$

where A_t is the flow area (m^2), ε is the porosity, r_{zi} the reaction rate for component i at the position z (kmol s^{-1} kg^{-1}) and $\alpha_{i,j}$ is the stoichiometric coefficient for component i, within the reaction j.

The reformer heat duty for each operational condition is rigorously calculated using local film coefficients information and the overall heat transfer coefficient definition (Eq. (11)) [7,25]:

$$Q = UA_{tc}(T_g^{in} - T_g^{out}) \quad (11)$$

here Q is the heat duty (kW), A_{tc} the heat transfer area (m^2) and U is the overall heat transfer coefficient (kW m^{-2} K^{-1}).

The reactor is supposed to be operated near isothermal conditions, and the energy to drive the endothermic reactions is controlled by external heating through the tube wall, the main geometrical parameters are showed in a previous work [7]. Temperature and water/ethanol molar ratios are considered as the most important variables in the analysis based upon previous results reported elsewhere [5–7,22,23]. The fuel utilization coefficient is also considered in the study due to the dual influence of this parameter in the system efficiency: high levels of (FUC) favor the power output reducing the energy content in the cell off gases. On the other hand, lower fuel utilization allows obtaining a fuel cell off gas with a higher LHV, increasing in that way the heat recovery and the auto-sustainability of the system.

2.3. Solid oxide fuel cell

A generalized steady-state model is used [7,26–27] in order to investigate the performance of a SOFC coupled to an ESR reactor. A high operation temperature (923 K) is chosen in order to favor the in-situ reforming reactions and to increase the energy content of the exhausted gas. The anode (rich in steam) and cathode (air rich N_2) depleted gases are mixed and fed into a post-combustion unit. The synthesis gas (enter to the anode) contains mainly H_2, CH_4, CO, CO_2, H_2O and due to this the common internal methane reformer is considered. The operation temperature is maintained using a flowing air stream.

A simple SOFC model represented in Fig. 2 is used to study the process and to design the heat exchanger network. The methane reforming reaction is studied using a conversion reactor (RStoic) modeled in Aspen Plus. The air and fuel flows are brought to operating temperature using (Heatx) blocks. The oxygen consumed in the electrochemical reaction (Eq. (12)) is separated from the air using a (Separator) block and the inlet flow of air is calculated for an oxygen stoichiometry of 2, representing a utilization of 50% [3]. The anode reaction is evaluated using a (RStoic) reactor model and varying the fuel utilization coefficient defined by (Eq. (13)) between 70 and 90%. The heat balance in the cell considers the heat consumed in the methane reforming and the heat produced by the electrochemical reaction.

$$H_2 + \tfrac{1}{2}O_2 \rightarrow H_2O \quad (12)$$

$$FUC = \frac{(f_{H_2}^{in} + X_{CH_4} \times f_{CH_4}^{in} - f_{H_2}^{out})}{(f_{H_2}^{in} + X_{CH_4} \times f_{CH_4}^{in})} \quad (13)$$

where f_{in}, f_{out} are the molar flows entering and leaving the fuel cell ($kmol^{-1}$). The X_{CH_4} is the methane conversion for the in-situ steam reforming.

The total cell stack current and the equilibrium voltage (V_{ideal}) are calculated assuming the principles depicted in Francesconi et al. [9] and the Nerst equation (Eq. (15)). The reforming reaction is considered to be much faster than the electrochemical oxidation of CO and CH_4; this is justified by the high content of water in the reforming gas and the operational conditions within the fuel cell, a more detailed analysis should consider the kinetics of the in-situ methane reforming on the fuel cell performing:

$$I_{cell} = 2F[(f_{H_2}^{in} + X_{CH_4} \times f_{CH_4}^{in}) - f_{H_2}^{out}] \quad (14)$$

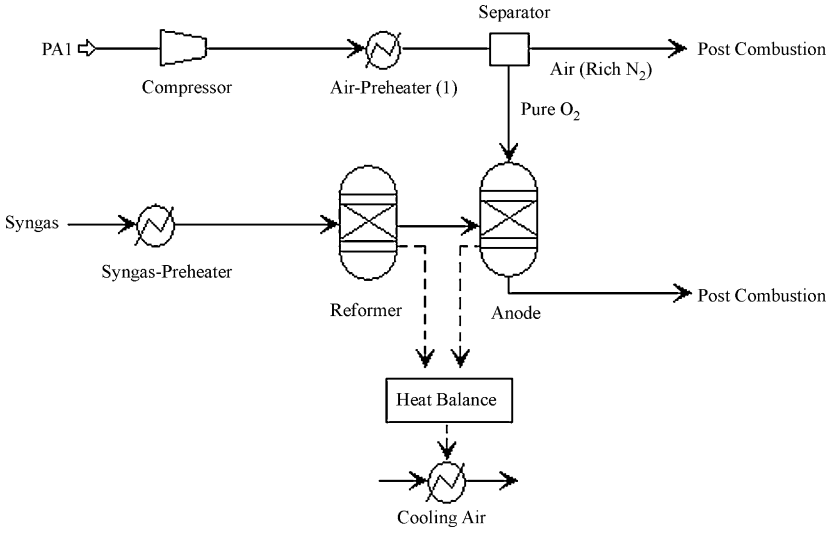

Fig. 2. Solid oxide fuel cell. Model scheme.

$$V_{ideal} = \frac{-\Delta G}{nF} + \frac{RT}{nF} \ln\left(\frac{p_{H_2} \cdot p_{O_2}^{0.5}}{p_{H_2O}}\right) \quad (15)$$

The molar free energy change is calculated at the cell operation temperature and pressure. All partial pressures are average values between the inlet and outlet of the anode and cathode, respectively.

Other important parameter is the current density (J) and is calculated for an active cell surface (S_{SOFC}) of 100 m^2.

$$J = \frac{I_{cell}}{S_{SOFC}} \quad (16)$$

The actual cell voltage (V_{cell}) and power (P_{cell}) are estimated using the V_{ideal} defined above and considering the irreversibility losses which mainly occurs due to concentration, activation and ohmic overpotentials.

$$V_{cell} = V_{ideal} - \eta_{act} - \eta_{conc} - \eta_{Ohm} \quad (17)$$

$$P_{cell} = I_{cell} V_{cell} \quad (18)$$

The activation overpotential is related to the electrode kinetics at the reaction site and the relationship between overpotential–current density can be expressed by the Butler–Volmer equation [27], which for a typical SOFC is expressed as [27,28]:

$$\eta_{act} = \left(\frac{RT}{F}\right) \sin\ h^{-1}\left(\frac{J}{2J_{o,i}}\right), \quad i = a,\ c. \quad (19)$$

This expression is valid when two electrons are transferred in the electrochemical reaction, the symmetric factor of the SOFC (alpha) is 0.5 and could vary if the oxidations of CH_4 and CO are considered [27,29].

Experimental results have demonstrated the influence of the operational parameters on the exchange current density (J_o) and the activation overpotentials at the cathode and anode in the SOFC. This relationship was described in Ni et al. [27] and used in the present paper to obtain the real output power of the SOFC when the FUC is varied:

$$J_{o,a} = \left(\frac{P_H}{P_{ref}}\right)\left(\frac{P_{H_2O}}{P_{ref}}\right) \exp\left(\frac{-E_{act,a}}{RT}\right) \quad (20)$$

$$J_{o,c} = \left(\frac{P_{O_2}}{P_{ref}}\right) \exp\left(\frac{-E_{act,c}}{RT}\right) \quad (21)$$

here $J_{o,a}$ and $J_{o,c}$ are the anode and cathode current densities, P_i are the partial pressures of chemical species, P_{ref} is the reference pressure, hydrogen oxidation activation energy $E_{act,a}$ (1.0×10^5 J mol^{-1}) and oxygen reduction activation energy $E_{act,c}$ (1.2×10^5 J mol^{-1}).

On the other hand, the concentration overpotential is evaluated considering the limit current density, defined by Wang [30]. This parameter is closely related to the transport properties of the fuel and oxidant and the morphological characteristics of the cell electrodes:

$$\eta_{conc} = \frac{RT}{nF} \ln\left(1 - \frac{J}{J_l}\right) \quad (22)$$

The effect of the Ohmic overpotential on the cell voltage is calculated using the equation presented by Ni et al. [27], it is only affected by the electrolyte properties, the temperature and the current density within the cell.

2.4. Post-combustion unit

The SOFC exhaust containing H_2, CH_4, O_2, N_2, CO, H_2O, and CO_2 is cooled (to avoid NO_x formation) and burned downstream in the post-combustion system. The produced heat is used to balance the energy requirements in the process. Supplementary firing of ethanol must be considered if the energy content of the depleted fuel is not enough to close the balance. A heat integration technique allows avoiding the ethanol needs and designing the heat exchanger network which better fit the energy requirements in the system.

The energy recovery depends of various factors:

- The exhaust temperature and composition.
- Fuel utilization coefficient in the SOFC.
- Air excess in the burner.

The operational conditions (feed temperature, pressure and air excess) of the after burner are taken into account in the system analysis and the model considers four reactions:

$$H_2 + \tfrac{1}{2}O_2 \rightarrow H_2O$$

$$C_2H_6O + 3O_2 \rightarrow 3H_2O + 2CO_2$$

$$CO + \tfrac{1}{2}O_2 \rightarrow CO_2$$

$$CH_4 + 2O_2 \rightarrow CO_2 + 2H_2O$$

2.5. Heat exchange model using PINCH technology

The opportunities of energy savings in the plant are calculated using the PINCH technology approach. The method is applied in two general steps:

- A targeting phase that aims identifying energy requirements of the system considering the heat recovery between hot and cold streams.
- Design of the optimal heat exchanger network (HEN).

This method has been applied partially to study other fuel cell schemes and processes with intensity in the heat consumption [10–12,19]. In order to start the Pinch Analysis the necessary thermal data are extracted from the process flow diagram. Using the base case simulation architecture depicted in Fig. 1, the heat and mass balances in all process units are carried out and data extraction is developed subsequently. The streams defined as hot and cold represents the heat sources and sinks, respectively.

The temperature–enthalpy (T–H) profiles of heat availability in the process (the "hot composite curve") and heat demands (the "cold composite curve") are used together in a graphical representation to calculate the minimum energy targets in the system.

The minimum temperature approach for overlapping the energy curves (hot and cold) is fixed at 40 K. This value should change in the optimization procedure in order to reduce the heat exchanger area and cost.

3. Quantitative parameters

The process effectiveness and efficiencies are computed using different criteria:

1. *Steam reforming reaction*.
   - Hydrogen yield and selectivity (Y_H, S_H).
   - Reaction efficiency (η_{ref}).
2. *Energy efficiency*.
   - Fuel cell (η_{cell}).
   - Reforming (η_{esr}).
   - Total system (η_{syst}).

Selectivity towards hydrogen is calculated taking into account the variation of ethanol and water concentrations (Eq. (23)); and the reaction efficiency is defined as the ratio of H_2 actual molar flow and

the maximum molar flow obtained under equilibrium conditions (Eq. (24)).

$$S_H = \frac{F_H}{[3(F^{in}_{ethanol} - F^{out}_{ethanol}) + (F^{in}_{water} - F^{out}_{water})]} \quad (23)$$

$$\eta_{ref} = \frac{F_H}{f^{Eq}_{H_2}} \quad (24)$$

Energy efficiency in the SOFC is evaluated by the ratio of fuel cell electric power and the energy that could be produced if the hydrogen entering into the cell is completely burned:

$$\eta_{cell} = \frac{P_{cell}}{(f^{in}_{H_2} + X_{CH_4} \times f^{in}_{CH_4})LHV_{H_2}} \quad (25)$$

A similar criterion was used by Perna [12]. At this calculation stage the heat removed from the cell is not considered as a hot source and the cost of utilities in the system is affected by the cooling air price. This could lead with a different HEN design, but is a very good alternative considering that high flows of air are needed for the fuel cell conditioning. Another way to solve this question is to use the air to develop a cogeneration scheme.

The reforming and the total system efficiencies are related only to the produced and consumed energy in the main process equipments, but are also affected by the energy needs in the auxiliary equipment (pumps and compressors). The steam reformer efficiency is computed as the ratio between the LHV of hydrogen leaving the reactor and the LHV of the total ethanol entering into the system (reforming and post-combustion stages).

$$\eta_{esr} = \frac{F_{H_2} LHV_{H_2}}{[(f^{in}_{ethanol} + f^{Post\text{-}comb}_{ethanol})LHV_{ethanol}]} \quad (26)$$

$$\eta_{sys} = \frac{(P_{cell} - W_{comp} - W_{pumps})}{[(f^{in}_{ethanol} + f^{Post\text{-}comb}_{ethanol})LHV_{ethanol}]} \quad (27)$$

In the present paper a novel parameter allows calculating the heat recovery potential in the post-combustion unit: This parameter relates the proportional energy content of the exhaust gas with the energy demand of the vaporization, reheating, reforming and preheating stages:

$$HRP = \frac{(Q_{CH_4} + Q_{CO} + Q_{H_2})}{(Q_V + Q_{RH} + Q_{REF} + Q_{PRE})} \quad (28)$$

where Q_{CH_4}, Q_{CO}, $Q_{C_2H_6O}$ are the lower heating values multiplied by the mass flow of CH_4, CO and H_2 in the fuel cell exhaust (kW). Q_{REF}, Q_V, Q_{RH}, Q_{PRE} are the heats consumed in the reaction, vaporization, reheating and conditioning stages (kW).

4. Simulation results and discussion

In the upcoming sections, the effect of the main process variables on reaction and energy efficiencies is discussed. The variables are explored in the ranges as shown in Table 1.

4.1. SOFC results for operation with synthesis gas

The following results (Fig. 3) show the effect of the fuel utilization coefficient in the SOFC characteristic curves for a typical reformate gas composition (40%H_2, 37%H_2O, 2.5%CO, 13.8%CO_2 and 6.7%CH_4). The increments of the FUC results in a high activation and concentration losses, the Ohmic overpotential and the partial pressure of oxygen at the cathode outlet are slightly reduced. The combine effect of these factors allows the power produced by the SOFC to reach a maximum which coincides with lower utilization factors and high current densities values. On the other hand, the heat recovery potential diminishes with the FUC due to the lower hydrogen content in the cell off gasses, affecting in that way the energy balance of the system; due to this when the SOFC runs at FUC < 0.7, the electric efficiency falls and makes the system unsustainable from the energy point of view and the coke deposition within the cell electrodes is more critic [16] (see Section 5.1).

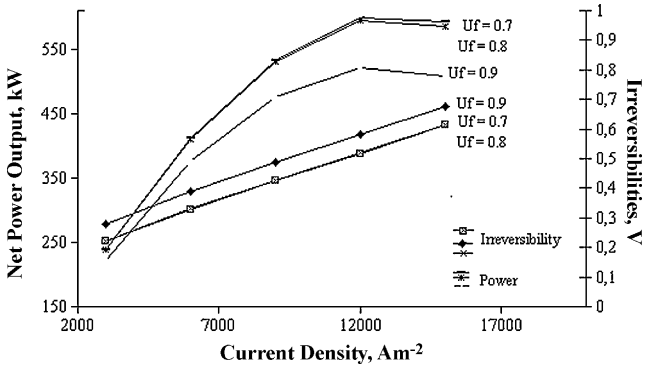

Fig. 3. Effect of the fuel utilization factor on irreversible losses and power production in a SOFC.

4.2. Effect of water/ethanol molar ratio

The influence of Water/ethanol molar ratio on ethanol steam reforming process (vaporization + heating + reforming) follows the basic principles of thermodynamic and heat transfer: An increment of water content causes a direct change of the boiling point and the total flow, and due to this the energy needs in the vaporization stage rises abruptly. More over, this factor is proportional to the energy consumption (sensitive heat) in the heating, reforming and reheating stages, respectively. Figs. 4 and 5 show more clearly the issues of the energy consumption in an ESR–SOFC system.

Values in Fig. 4 show the ratio between the Q_{CH_4}, Q_{CO} and $f^{out}_{H_2} \times LHV_{H_2}$ in the fuel cell exhaust, the heats consumed in the reaction, vaporization, reheating and conditioning stages and the LHV content of the hydrogen produced in the reforming stage (kW/kW). The vaporization and heating stages require 65.21% of the produced hydrogen HHV, this result agrees with the high energy consumption factor of the steam reforming processes and clearly justify the HEN integration analysis developed in the present paper.

Moreover, the water/ethanol molar ratio favors the reaction efficiency (see Fig. 6). While R_{AE} is increased from 3 to 5.5 the efficiency is favored, from this point forward the curve slope changes due to the process thermodynamic limitations, accordingly to Diagne [31,26] its expected that this tendency becomes worse for $R_{AE} > 8$, and at lower temperatures this effect is less important. While the water to ethanol molar ratio is increased the methane reforming equilibrium is favored (Le Châtelier–Braun principle) as well in the reactor as the fuel cell electrodes; due to this the potential for energy recovery by CH_4 combustion is strongly reduced.

The energy efficiencies are also affected by the ethanol dilution in the reacting mixture, the impact on reforming efficiency (η_{esr}) is more drastic than the other efficiency criteria (Fig. 7). A η_{esr} variation of 14.65% occurs when water content varies from 3 to 6, due to the increment in the H_2 yield. The fuel cell and total efficiencies are stable at the studied R_{AE}, the cell efficiency suffers a slight decrease due to the methane reforming at the reactor. The weak

Table 1
Range of the independent variables.

Variable	Value	U/M
Temperature	723–873	K
Water/ethanol molar ratio	3–6	mol H_2O/mol EtOH
Fuel utilization coefficient	0.7–0.9	mol H_{2in}/mol H_{2out}

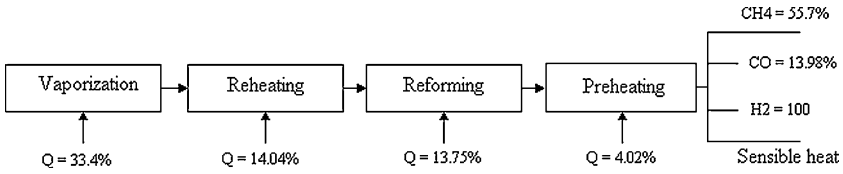

Fig. 4. Distribution of heat use in the ESR–SOFC system. T = 823 K, P = 1 atm, R_{AE} = 5.

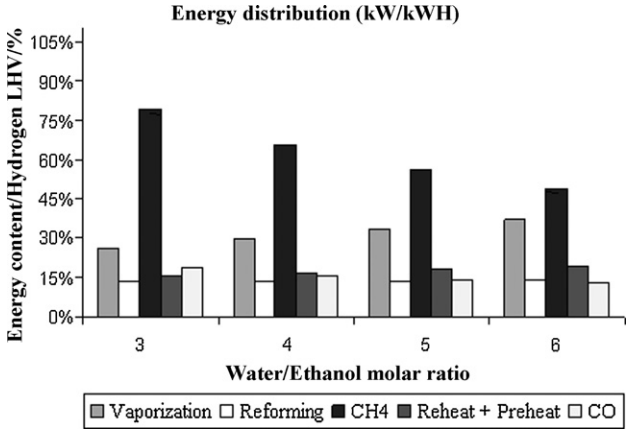

Fig. 5. Influence of R_{AE} on energy distribution in an ESR–SOFC system. T = 823 K and P = 1 atm.

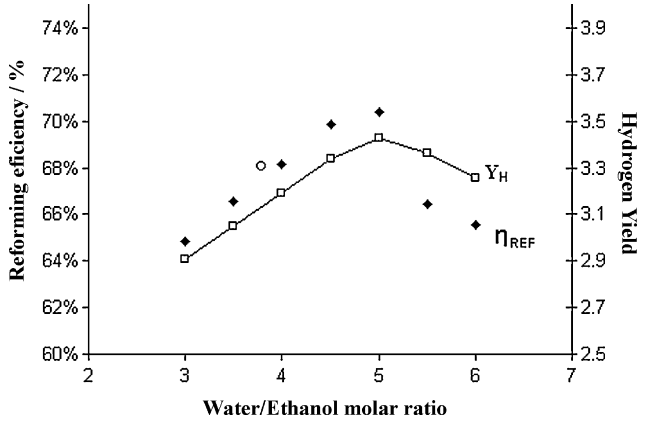

Fig. 6. Water/ethanol molar ratio influence on reforming efficiency and hydrogen yield. T = 823 K.

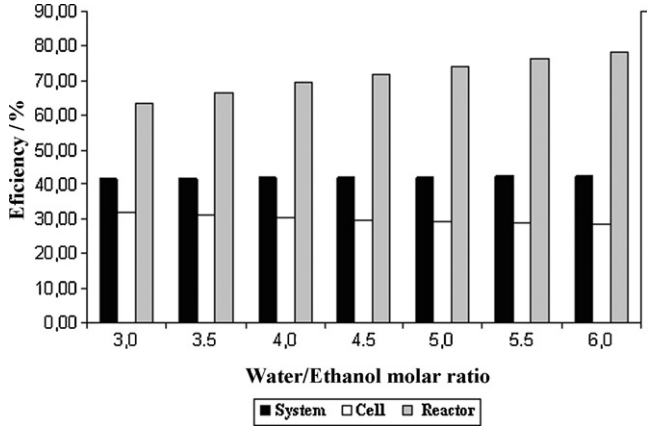

Fig. 7. Water/ethanol molar ratio effect on the energy efficiencies. T = 823 K, P = 1 atm.

effect of water content in the cell efficiency is closely related with the activation and concentration losses in the electrodes, which are increased with the increment of water partial pressure. On the other hand, the partial pressure of water makes a reduction of the Nerst potential (see Eq. (15)) lowering in that way the produced power and compensating the positive effect of hydrogen content in the reformate gas.

Summarizing the discussed above, can be stated that the water content:

- Increases the reaction yield, and the energy efficiency in the reformer.
- Increases the heat consumption at the conditioning stages.
- Superimposes a higher exhaust reuse.
- Favors the equilibrium of methane reaction at the reformer.

When the partial pressure of water at the reactor inlet is increased, HRP is reduced. The kinetic model reveals clearly the relationship between these factors, because the steam reforming reactions are favored, the conversion of CH_4 to hydrogen increases producing a proportional reduction in the energy content of the fuel leaving the reactor and fuel cell electrodes, respectively. The equilibrium of the HRP is placed at R_{AE} = 5.35 (Fig. 8).

4.3. Effect of the reaction temperature

The temperature favors the steam reforming reaction efficiency and selectivity of H_2 (see Fig. 9). When the reactor temperature is increased the methane steam reforming (Eqs. (6) and (7)) and the ethanol decomposition (Eq. (4)) reactions are favored conducting to higher hydrogen content in the synthesis gas stream. The carbon monoxide production rises slightly when the temperature overcomes the 823 K because of the reverse water gas reaction (RWGSR), but the levels of hydrogen production justify developing the reaction at these high temperatures. The SOFC fuel cell runs properly at the existing CO concentration (CO <5%mol) when temperature is up to 823 K and the HHV of the gasses leaving the cell electrodes is increased, in that way the remaining CO can be burned in the

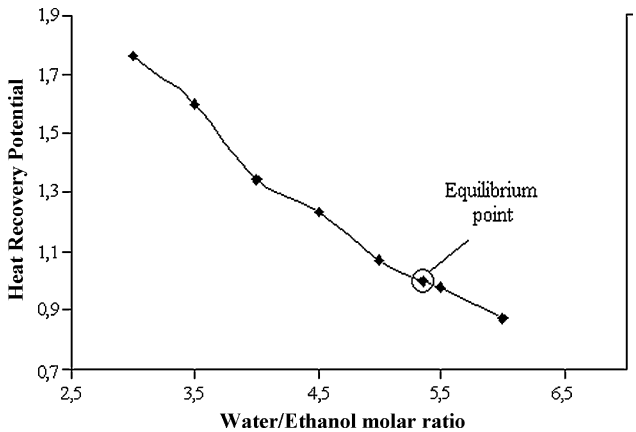

Fig. 8. Effect of water/ethanol molar ratio on the heat recovery potential. P = 1 atm, T = 823 K, FUC = 80%.

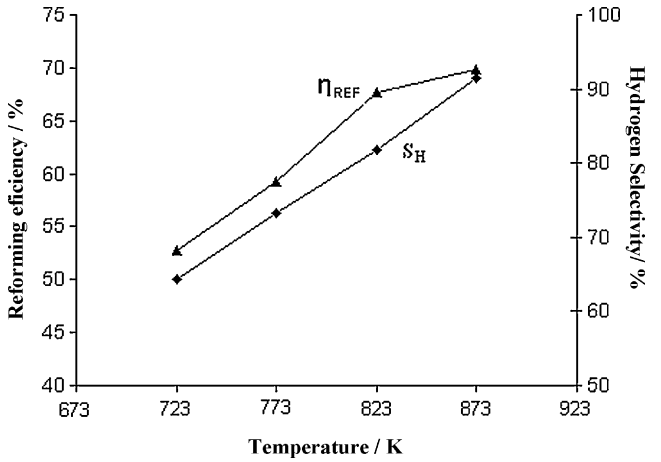

Fig. 9. Effect of temperature on reaction efficiency and hydrogen selectivity. $R_{AE} = 5.5$, $P = 1$ atm.

post-combustion unit to fulfill the energy requirements in the process. The fuel cell efficiency is increased with temperature, although when the 823 K is surpassed, this behavior is less important and the fuel use $(1 - (LHV_{in}/LHV_{out}))$ fall, due to the in-situ RWGSR.

On the other hand, if the temperature surpasses the 823 K and if the ethanol to water molar ratio is controlled above 1:3 the carbon gasification is favored and the catalyst deactivation is reduced, considering that this is one of the most important limitations of the reforming catalysts in this work the process synthesis and integration is carried out for a reforming reactor running at 823 K and 1:5.5 ethanol to water molar ratio.

The low heat transfer efficiency of reforming processes [18] at high temperatures requires a heat recovery system which depends of the synthesis gas composition and the fuel utilization in fuel cell. All the results presented above justify the needs of energy integration to obtain a real auto-sustained and green, energy production system.

5. Heat integration

On the basis of the result obtained, the synthesis of the process is continued. As it was mentioned before, the procedure is composed of two steps:

1. Targeting of the base process.
2. Design of the optimal heat exchanger network.

In the step 1 the FUC coefficient is varied from 70 to 90%, when FUC is up to 80% the necessary extra ethanol is null and the system operates properly without any external source of energy. The previously mentioned allows to state that the net CO_2 contribution is near to cero because all the oxide molecules come from bio-resources which can assimilate it in a relative short time.

The feasibility to carry out the energy integration for the hydrogen catalytic production and SOFC fuel cell, using ethanol as raw material is demonstrated, with total energy efficiencies η_{ref} ranging 63–78% and η_{syst} 41–45%. These efficiencies must include energy losses (heat loss in tubing or reformer furnace, Joule effect, electrical motor intrinsic efficiency).

5.1. System targeting

The stream data, heat flows, heat exchanger areas and cost laws of the base process are shown in Table 2.

Five cold and three hot streams exist in the heat exchanger network of the process, the liquid mixture is dived into four segments

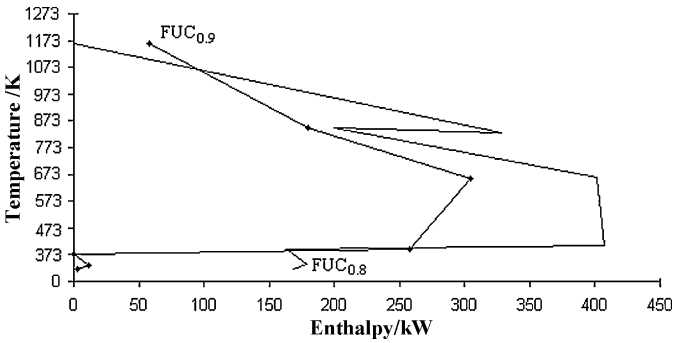

Fig. 10. Grand Composite Curve for FUC = 90% and FUC = 80%.

to study the nonlinear behavior of the vaporizing curve. The temperature of the fuel cell off gasses is controlled to avoid the formation of NO*x* in the after burner. In this way, part of the energy content of this stream is used to preheat cold sinks and the damage to the environment is reduced.

Hot utility (low pressure flue gas) and cold utility (cooling air) are necessary when FUC is up to 90%, see Grand Composite Curve (Fig. 10), target minimum hot utility flow at these conditions is 58.1 kW and the cold one 3.2 kW, plus the fuel cell cooling air (906.4 kW air). However, when FUC is 80% or less, hot utility is not required and 169.3 kW of cooling air are necessary to balance the system (Fig. 10) without the integration with the cell cooling system. The influence of the composition of the exiting gasses leaving the fuel cell on the energy balance of the HEN is very important. While the FUC decreases a higher recovery of heat in the after burner is possible but the cell efficiency and the output power are reduced, because of this the feasible FUC is fixed at 80%.

At this condition the energy curve remains flat in a wide range of ΔT_{min} and the threshold process condition is reached avoiding the need of a utility optimization procedure.

If the heat released by the fuel cell is used in a low temperature cogeneration system, the total efficiency can be increased drastically.

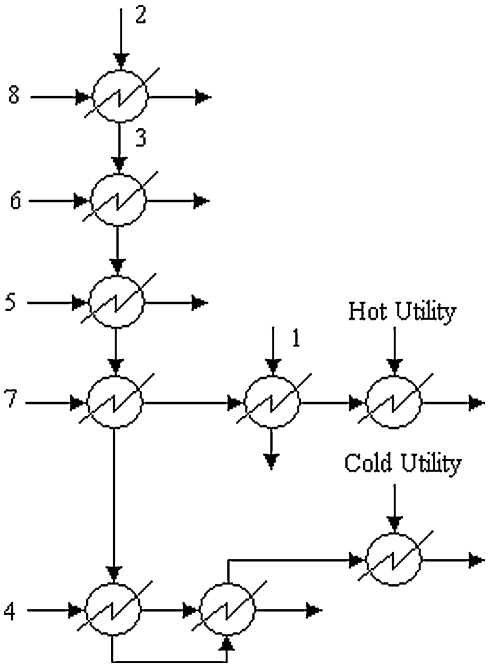

Fig. 11. Heat exchanger network for FUC = 90%.

Table 2
Process data used for heat integration. R_{AE} = 5, FUC = 80%, P = 1 atm.

No.	Type	Description	T^s (K)	T^t (K)	C (kW K^{-1})	Q (kW)
1	Hot	Fuel cell exhaust	923	673	1.0523	263.06
2	Hot	Burner exit gases	1181.16	1067.25	1.1253	128.18
3	Hot	Burner exit gases	1067.25	353	1.0212	729.38
4	Cold	Liquid mixture to vaporize	298	333	0.5326	18.64
4	Cold	Liquid mixture to vaporize	333	256.72	0.5761	13.6633
4	Cold	Liquid mixture to vaporize	256.72	373	16.556	269.576
4	Cold	Liquid mixture to vaporize	373	413	0.2733	10.934
5	Cold	Vapors to be heated	413	823	0.3158	129.49
6	Cold	Synthesis gas to SOFC	823	923	0.3745	37.5
7	Cold	SOFC oxidant	370.17	873	0.6831	343.47
8	Cold	Reactor duty	823	823	–	128.18

Utility		Economic data			hi kW (m^2 K)$^{-1}$	Cost US$ (kWh)$^{-1}$
U1	Hot	Flue gas	1173	673	1.2–4	0.21
U2	Cold	Air	298	313	0.08–0.12	0.129
Heat exchanger cost ($)		$1212.8 \times A^{0.075}$ $1855.8 \times A^{0.6375}$	$A < 9$ m^2 $9 < A < 500$ m^2			Ref. [32]

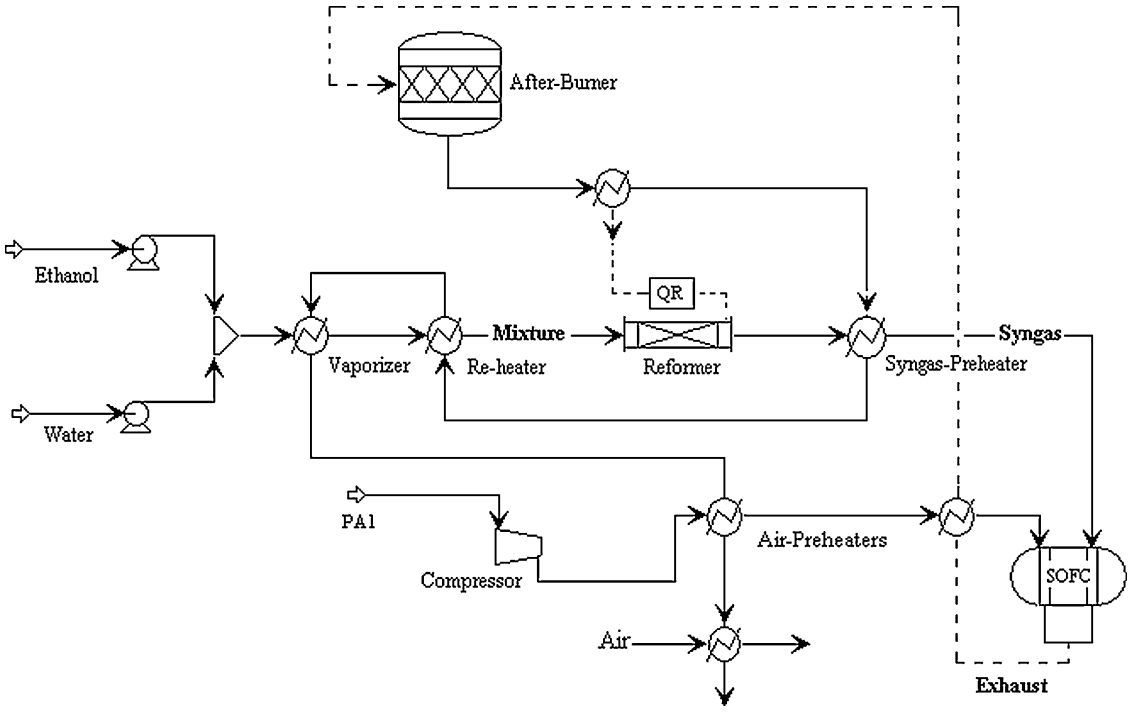

Fig. 12. Integrated process flow diagram.

5.2. Heat exchanger network design

A countercurrent arrangement between hot and cold sources is used to calculate the MLDT and the heat exchanger area. The heat exchanger network scheme for FUC = 90%, is represented in Fig. 11, nine heat exchangers exist in this network with a total heat transfer area of 251.7 m^2. An extra 0.17 kmol h^{-1} of ethanol are required to produce the supplementary heat of the system (hot utility), con-

Table 3
Design details of the HEN for FUC = 80% and total reuse of fuel cell exhaust.

Parameter	Symbol	Value	U/M
Heat exchangers	Nic	7	–
Total network area	$A_{tc_{RIC}}$	213.6	m^2
Investment cost	CTI_{RIC}	100397.14	USD$
Utility cost	C_{en}	157248.7	$/a
Total annualized cost	CTA_{RIC}	25763.59	$/a
Design parameters/pinch results			
Used utility/minimum required	$Q_{cold}/Q_{MIN\text{-}cold}$	1	kW/kW
Used area/minimum required	$A_{tc_{RIC}}/A_{tc_{MIN}}$	1.37	m^2/m^2
Used area for utility HEx/minimum required	Au_{real}/Au_{MIN}	1.01	m^2/m^2

sidering an ethanol lower heating value of 1.2335×10^6 kJ kmol^{-1}. This extra ethanol firing is a clear limitation which reduces the system auto-sustainability and affects the total efficiency. The ratio between the area of the installed units and the minimum area requirements is 1.05 at the condition of minimum utility load.

If a comparison between the HEN for 80 and 90% is done, can be realized the profit of running the process at FUC of 80%, where the annual cost of utilities is about 17.84% of that calculated for a FUC = 90%. Also, when FUC = 90% the HEN requires two more heat exchangers to fulfill the area requirements and the pinch constraints, increasing in that way the total annualized cost.

The process flow diagram considering a total reuse of cell exhaust, 80% of FUC, a reforming temperature of 823 K and at atmospheric pressure is represented in Fig. 12. Table 3 presents the main characteristics of the designed HEN.

6. Conclusions

The presented model allows describing the performance of a stationary SOFC–reforming system fueled by ethanol. The ethanol reforming reactor was studied considering a detailed kinetic model and the system efficiencies are evaluated considering the effect of water content in the reacting mixture and the reforming temperature.

The impact of the FUC was described and a dual effect is presented: when FUC is 80% the system is totally balanced and no external source of energy is required helping in that way to establish a CO_2 closed loop.

Two heat exchanger networks were designed being demonstrated that when the fuel utilization coefficient in the SOFC is 80%, the reforming reactor temperature 823 K and the ethanol to water molar ratio 1:5.5 the auto-sustainability condition is reached.

It was also demonstrated that an efficient ethanol processor not only depends on the reaction but also depends on well designed heat exchanger network and process integration.

Acknowledgments

The authors whish to acknowledge to editor and unknown referees. Arteaga acknowledges the professor Miguel Laborde, the researchers of the Catalytic Productions Laboratory of Universidad de Buenos Aires and the CYTED (Projects 3303 & 332205).

References

[1] B. Thorud. Dynamic modelling and characterization of a solid oxide fuel cell integrated in a gas turbine cycle. Doctoral Thesis. Department of Energy and Process Engineering, Norwegian University of Science and Technology, 2005.
[2] Ballard, Case Study—Residential Cogeneration. Groundbreaking Fuel Cell Solution, Ballard Power Systems Inc., 9000 Glenlyon Parkway Burnaby, British Columbia, 2007.
[3] J.H. Hirschenhofer, D.B. Stauffer, R.R. Engleman, M.G. Klett, Fuel Cells Handbook, sixth ed., EG & G Technical Services, National Energy Technology Laboratory, P.O. Box 880. Morgantown, West Virginia 26507-0880.
[4] S.D. Minteer, Alcoholic Fuels: An Overview. Sect. Application of Alcoholic fuels, Taylor and Francis Group, Copyright 2007.
[5] J. Comas, F. Marino, M. Laborde, N. Amadeo, Chem. Eng. J. 98 (2004) 61–68.
[6] M.A. Laborde, Producción y Purificación de Hidrógeno a partir de Bioetanol y su aplicación en pilas de combustible, CYTED (2006), ISBN: No. 987-05-1795-1.
[7] L.E. Arteaga, L.M. Peralta, V. Kafarov, Y. Casas, E. Gonzales, Chem. Eng. J. 136 (2008) 256–266.
[8] J. Sun, X.P. Qiu, F. Wu, W.T. Zhu, Int. J. Hydrogen Energy 30 (2005) 437–445.
[9] J.A. Francesconi, M.C. Mussati, R.O. Mato, P.A. Aguirre, J. Power Sources 167 (2007) 151–161.
[10] P. Giunta, C. Mosquera, N. Amadeo, M. Laborde, J. Power Sources 164 (2007) 336–343.
[11] J. Godat, F. Marechal, J. Power Sources 118 (2003) 411–423.
[12] A. Perna, Int. J. Hydrogen Energy 32 (2007) 1811–1819.
[13] S.L. Douvartzides, F.A. Coutelieris, P.E. Tsiakaras, J. Power Sources 114 (2003) 203–212.
[14] S.L. Douvartzides, F.A. Coutelieris, P.E. Tsiakaras, J. Power Sources 131 (2004) 224–230.
[15] P. Tsiakaras, A. Demin, J. Power Sources 102 (2001) 210–217.
[16] M. Cimenti, J.M. Hill, J. Power Sources 186 (2009) 377–384.
[17] S. Song, S. Douvartzides, P. Tsiakaras, J. Power Sources 145 (2005) 502–514.
[18] S. Kiende, M. Seidel, Integrated Chemical Processes. Synthesis, Analysis and Control, Wyley-VCH, Verlog Gans Co KGaA, 2003.
[19] M. Krajnc, A. Kovac-Kralj, P. Glavic, Appl. Thermal Eng. 26 (2003) 881–891.
[20] V. Fierro, O. Akdim, H. Provendier, C. Mirodatos, J. Power Sources 145 (2005) 659–666.
[21] I. Fishtik, A. Alexander, R. Dattaa, D. Geanab, Int. J. Hydrogen Energy 25 (2000) 31–45.
[22] M. Laborde, E.Y. Garcia, Int. J. Hydrogen Energy 16 (1991) 307–317.
[23] V. Mas, G. Baronetti, N. Amadeo, M.A. Laborde, Chem. Eng. J. 138 (2008) 602–607.
[24] F. Mariño, M. Boveri, G. Baronetti, M.A. Laborde, Int. J. Hydrogen Energy 29 (2004) 67–71.
[25] R.H. Perry, D.W. Green, Chemical Engineers Handbook, sixth ed., McGraw-Hill Companies Inc., 1999.
[26] J.M. Smith, Ingeniería de la Cinética Química, sixth ed., ISBN-0-07-058710-8.
[27] M. Ni, M.K. Leung, D.Y. Leung, Energy Convers. Manage. 48 (2007) 1525–1535.
[28] S.H. Chan, Z.T. Xia, J. Appl. Electrochem. 32 (2002) 339–347.
[29] F. Calise, A. Palombo, L. Vanoli, J. Power Sources 158 (2006) 225–244.
[30] J. Wang, Analytical Electrochemistry, second ed., John Wyley & Sons, 2000.
[31] C. Diagne, H. Idriss, K. Pearson, M. Gómez-García, A. Kiennemann, C. R. Chim. 7 (2004) 612–622.
[32] A. Jiménez, Diseño de procesos en Ingeniería Química, México 2003, Ed. Reverté S.A., 2003.